

Article

The Influence of a Surface Treatment of Metallic Titanium on the Photocatalytic Properties of TiO₂ Nanotubes Grown by Anodic Oxidation

Živa Marinko ^{1,2,*} , Luka Suhadolnik ¹ , Zoran Samardžija ¹, Janez Kovač ³ and Miran Čeh ¹

¹ Department for Nanostructured Materials, Jožef Stefan Institute, Jamova 39, 1000 Ljubljana, Slovenia; luka.suhadolnik@ijs.si (L.S.); zoran.samardzija@ijs.si (Z.S.); miran.ceh@ijs.si (M.Č.)

² Jožef Stefan International Postgraduate School, Jamova 39, 1000 Ljubljana, Slovenia

³ Department of Surface Engineering, Jožef Stefan Institute, Jamova 39, 1000 Ljubljana, Slovenia; janez.kovac@ijs.si

* Correspondence: ziva.marinko@ijs.si; Tel.: +386-1-4773-931

Received: 16 June 2020; Accepted: 16 July 2020; Published: 19 July 2020



Abstract: Titanium dioxide (TiO₂) nanotubes obtained by the anodic oxidation of titanium metal foils can be used for the photocatalytic degradation of organic pollutants. The aim of our study was to determine the influence of the titanium foil's surface treatment on the final morphology of the TiO₂ nanotubes and their photocatalytic activity. In our experiments, we used two different titanium foils that were electropolished or untreated prior to the anodic oxidation. The morphologies of the starting titanium foils and the resulting TiO₂ nanotube layers were investigated and the photocatalytic activities measured by the decomposition of caffeine under UV irradiation. Our results showed that electropolishing of the starting foils produced a more uniform and smoother TiO₂ nanotubes surface. In contrast, the TiO₂ nanotube surfaces from untreated titanium foils mimic the initial surface roughness of the titanium foil. A comparison of the photocatalytic properties of the TiO₂ nanotube layers obtained from the untreated and electropolished titanium foils showed that electropolishing does not necessarily improve the photocatalytic properties of the resulting TiO₂ nanotube layer. It was found that the determining factors influencing the photocatalytic activity are the chemical impurities (Ti-nitride) on the surface of the titanium foils and the surface roughness of the TiO₂ nanotube layer. The highest photocatalytic activity was achieved with the anodized untreated foil with the minimal presence of Ti-nitride and a relatively high roughness of the TiO₂ nanotubes.

Keywords: electropolishing; anodic oxidation; TiO₂ nanotubes; photocatalysis; metal titanium foil

1. Introduction

TiO₂ is a versatile, chemically inert, and low-cost photocatalyst that can decompose various organic pollutants with reactive oxygen species. The photocatalytic decomposition of the organic compounds starts with the absorption of photons with a suitable energy. It takes place in the presence of oxygen and consists of different chemical reactions, such as bond breakage and electron transfer/substitution. As a consequence, reactive oxygen species (ROS) are created [1,2]. The photocatalysis process takes place primarily at structural defect sites [3] or on the facets of the TiO₂ crystal with the highest surface energies [4–6].

TiO₂ anatase can be synthesized with a variety of approaches [7–11]. However, the anodic oxidation process is the most straightforward method for synthesizing TiO₂ nanotube arrays [12] due to the high degree of control over the nanotubes' morphology [7]. The driving force for the self-organized growth mechanism of the electrochemical oxidation process is the tendency to balance the formation of the oxide film and its dissolution in order to achieve the maximum nanotube density

on the titanium substrate [13]. The nanotubes formed during the anodization process are most often amorphous. In order to transform them into polycrystalline nanotubes, subsequent heat treatment at elevated temperatures is needed [14]. The obtained polycrystalline TiO₂ nanotubes are inherently intergrown into the metal substrate and thus represent a TiO₂ photocatalyst that can be directly used as a photocatalyst in immobilized photocatalytic or photoelectrocatalytic reactors [12,15]. Furthermore, an ingrown TiO₂ nanotube layer can provide a higher mechanical strength than a nanoparticulate film [16].

The formation and morphology of TiO₂ nanotubes are to some extent controlled by the titanium's surface topology, in particular by the surface roughness and the dislocation density [17,18]. These initial titanium surface artefacts influence the top surfaces of the TiO₂ nanotubes [19,20]. Additionally, a few-nm-thick oxide film forms spontaneously when the titanium foil is exposed to the air. The film is approximately 10 nm thick, amorphous, compact, chemically stable, and firmly adhered to the titanium foil [21]. It acts as a barrier and protects the titanium surface from corrosion.

The nanotubes' uniformity can be improved by (i) repeated anodization of the same substrate, after removing the anodized layer grown in the previous anodization [19] or (ii) with the polishing of the titanium surface, with mechanical, chemical or electropolishing techniques [17]. The process of electropolishing consists of three synergistic reactions: anodic dissolution, oxygen evolution, and the formation of a passive oxide film [22]. After applying a voltage between the titanium anode and the cathode, Ti⁴⁺ cations diffuse into the electrolyte. Active dissolution results in direct electropolishing of the titanium surface. Lee et al. [23] reported that the formation of electropolishing residues on the titanium surface have the ability to act as additional nucleation sites and at the same time lead to poor arrangements of the nanotubes due to the simultaneous activation.

In the present work, we studied the influence of the preparation of the titanium metal surface on the growth of TiO₂ nanotubes and their photocatalytic properties. Anodic oxidation of untreated and electropolished titanium foils from two different suppliers was performed to prepare photocatalytically active TiO₂ layers. The paper presents novel insights into the 'synthesis-properties-photocatalytic performance' relationships and reveals the main reason for the improvement or deterioration of TiO₂ photocatalytic properties with the titanium electropolishing procedure.

2. Results and Discussion

2.1. Characterization of the Titanium Metal Foils

Characterization of the titanium metal foils started with the grain size distribution analysis which influences the growth of TiO₂ nanotubes. In order to determine the grain size distribution of the starting titanium foils the electropolished foils were first chemically etched using hydrochloric acid and examined with optical microscope (see Supplementary Figure S1). Quantitative analysis of the grain size area revealed that the largest number of grains for the foil of Supplier 1 ranged between 10 and 30 μm², while for the foil of Supplier 2, the average grain area was around 100 μm². Smaller grains have a greater surface-to-volume ratio, which means more grain boundaries. Therefore, the titanium surface with a smaller grain size has a higher number of nucleation sites for the nanotube growth to occur [24]. The grain size analysis of untreated substrates could not be reliably conducted due to large surface roughness and present surface preferential deformations from cold rolling production. This is why the samples were electropolished and etched in order to reveal grain boundaries between different grains.

Observation of the titanium metal surfaces under field-emission gun scanning electron microscope (FSEM) revealed very different rolling patterns between the two suppliers: Supplier 1 showed straight and parallel lines, while the titanium foil of Supplier 2 exhibited random irregularities over the surface. In two studies, Zou and Wang [25,26] reported that the internal stress of a titanium foil influences the activity of local nucleation sites and therefore the nanotube growth. Baek et al. [27] additionally reported that deep valleys cause inhomogeneous deformation of the surface. These later lead to

various irregularities on top of nanotube oxide layer. The roughness factors, Ra (average arithmetical roughness), Rq (root-mean-square roughness), and Rt (peak-to-valley roughness), were measured on electropolished (190- μm -thick) and untreated (200- μm -thick) foils from both suppliers (see results in Supplementary Figure S2). Line scanning over an evaluation length of 4 mm of the sample was performed four times to determine the average value. Both untreated samples (Figure 1a,c) have a rough surface with cracks, pores, and scratches. Measurements showed that the average roughness is $0.161\pm 0.02\ \mu\text{m}$ for the sample of Supplier 1 and $0.168\pm 0.02\ \mu\text{m}$ for the sample of Supplier 2. Figure 1b,d shows the reduced surface roughnesses after the electropolishing, where the grain boundaries are also visible. The average arithmetical roughness decreased to $0.116\pm 0.01\ \mu\text{m}$ for the sample of Supplier 1 and to $0.123\pm 0.02\ \mu\text{m}$ for the sample of Supplier 2. It is interesting that the factor Rt is more prominent for the untreated sample from Supplier 2, which suggests that the specific analyzed surface area is larger than the untreated sample of Supplier 1. A closer look at the surface roughness of all the samples reveals that the specific surface area of the untreated titanium foils was higher than for the electropolished foils [24]. We also observed that electropolishing exposes the grain boundaries and causes the formation of pitting spots. They both influence the number of nucleation sites for nanotube formation, which affect the available active surface area for the photocatalytic reactions.

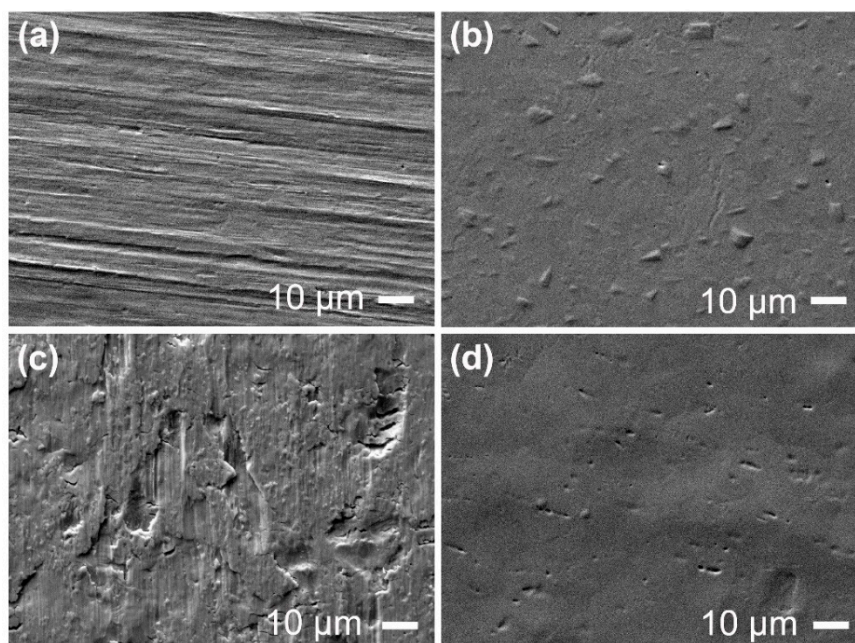


Figure 1. SEM images of metal titanium foil before and after electropolishing. (a) Untreated; (b) electropolished titanium foil from Supplier 1; (c) untreated and (d) electropolished titanium foil from Supplier 2.

Additionally, profilometry 3D mapping of a sample area of $1 \times 1\ \text{mm}^2$ was recorded. Statistical analyses with a Gaussian regression filter with standard values for both short (λ_s) and long (λ_c) cutoffs were calculated according to ISO 4287. Figure 2a,d presents the selective topographic results from the 3D surface roughness mapping. Although the difference in the z-axis was much smaller on the electropolished samples, the surface defects and shaping from the factory rolling remained visible. We also noticed some residues and undulations in the foil surface after the electropolishing, observed also by Jarosc et al. [28]. While the untreated titanium foil of Supplier 1 had an even distribution of peaks and valleys, different phenomena were observed on the untreated titanium foil from Supplier 2 (marked area in Figure 2c). Pits up to 5 μm deep surrounded with a series of peaks with a height of 4 μm were found on the foil. In detail, they are presented in Figure 2e (top and cross-section view).

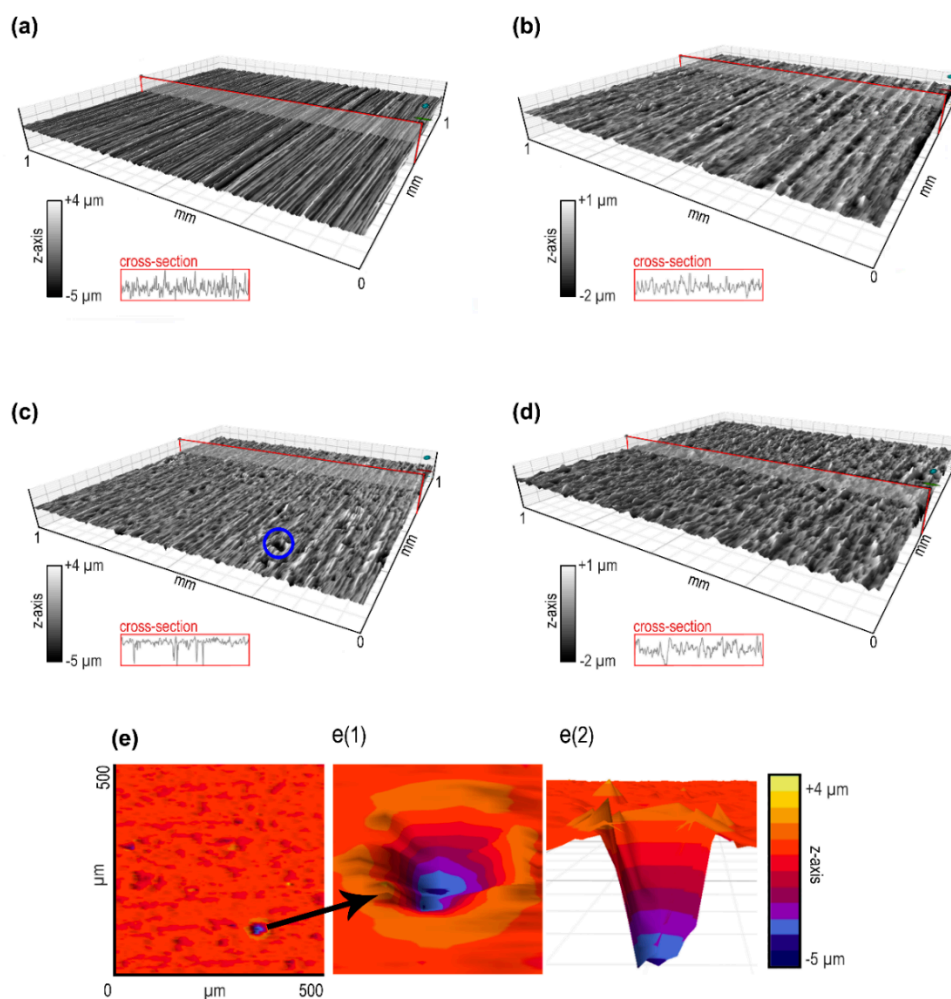


Figure 2. Profilometry 3D mapping of (a) untreated and (b) electropolished titanium metal foil from Supplier 1 and (c) untreated and (d) electropolished titanium metal foil from Supplier 2. The 3D mapping was measured on $1 \times 1 \text{ mm}^2$ surface. Each inset is showing a cross-section of the roughness profile. (e) Deep pit in the surface of titanium foil from Supplier 2, (e1) magnified area and (e2) cross-section image of the pit with z-axis legend.

As can be seen from the titanium foil's X-ray diffraction (XRD) patterns from both suppliers (see Supplementary Figure S3), the peak locations of both titanium foils overlap, however their relative intensities differ. The XRD peaks correspond to the hexagonal titanium crystal planes (100), (002), (101), (102), (110), (103), (112), (201), (004), (202), and (104). The diffractograms of our samples show the strongest peak intensities for the (103) crystal plane for Supplier 1 and (002) crystal plane for Supplier 2. Davepon et al. [29] reported that the crystallographic orientation of the titanium foil can be correlated to the electrochemical behavior. However, a recent study performed by Macak et al. [24] showed that grain orientation of the titanium foil does not play a significant role in promoting or retarding the growth of TiO_2 nanotubes in ethylene glycol electrolytes.

The surface chemistry was investigated using the X-ray photoelectron spectroscopy (XPS) method. The presence of Ti and O was revealed on the surfaces by the $\text{Ti } 2p_{3/2}$ peak at 458.6 eV and the $\text{O } 1s$ peak at 530.0 eV, indicating the TiO_2 -like surface oxide layer on all the samples [30]. In addition, surface contamination with carbon species ($\text{C } 1s$ at 284.8 eV) was found. The subsurface region between 0 and 10 nm in depth on all the samples was analyzed by XPS depth profiling. The obtained XPS depth profiles are shown in Figure 3. The thickness of the oxide layer was estimated from the XPS depth profiles as a depth at which the concentration curve for oxygen dropped to the half of its maximum

value. This is a rough estimation of the oxide thickness due to the limited depth resolution during XPS depth profiling related to not flat surface. They show that the untreated Ti foils were covered by a thin Ti-oxide film with a thickness of about 6 nm, while after electropolishing the oxide film was slightly thicker (7–8 nm). The main difference between the untreated metallic foils and the polished foils was in the presence of Ti-nitrides and Ti-carbides in the subsurface region. They were identified by the XPS spectra of N 1s at 397.0 eV and C 1s spectra at 282.0 eV, related to the nitrides and carbides [30]. As can be seen from Figure 3a,c, Ti-carbide and Ti-nitrides are present in the subsurface of the untreated sample of Supplier 1 (about 15 at.% of carbon and 2 at.% of nitrogen at a depth of 5 nm). In the subsurface region of the untreated sample of Supplier 2 a lower Ti-carbide concentration was found (about 12 at.% of C), but more Ti-nitride was present (about 10 at. %).

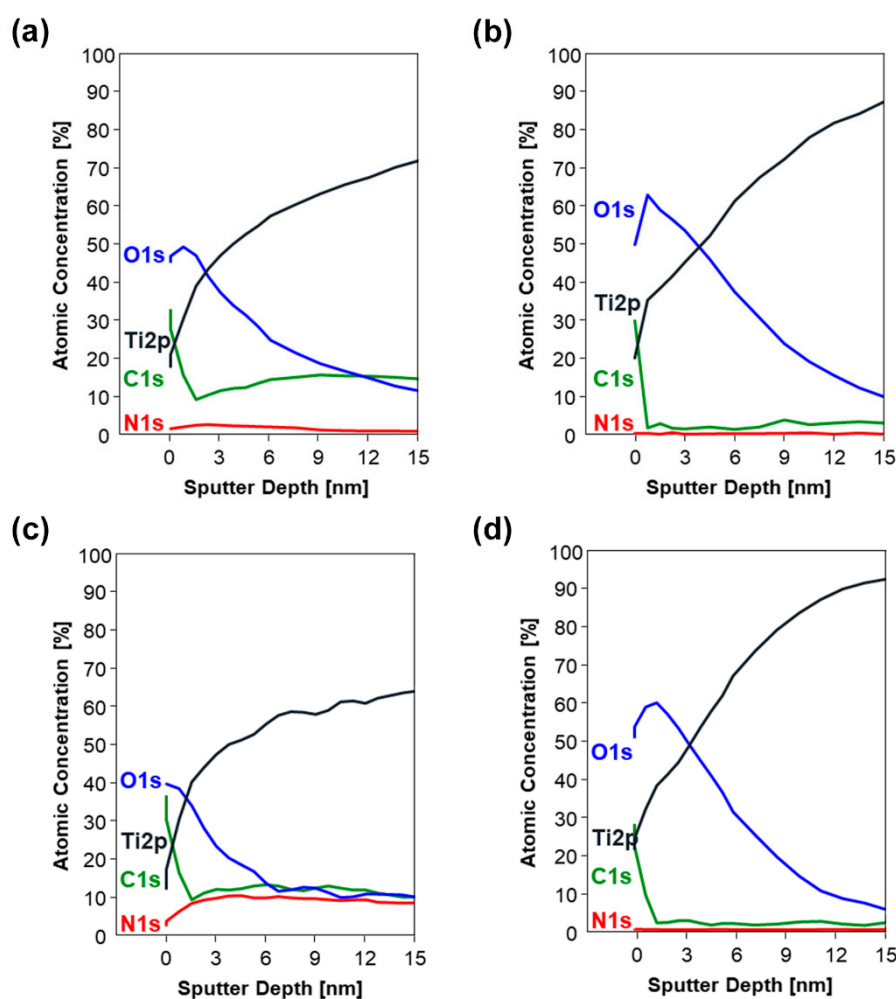


Figure 3. XPS depth profiling spectra for (a) untreated and (b) electropolished anodized samples from Supplier 1 and (c) untreated and (d) electropolished samples from Supplier 2. O 1s, Ti 2p, C 1s and N 1s peaks are marked.

2.2. Anodic Oxidation of the Titanium Foils

The current-time characteristics measured during the anodic oxidation of the differently treated titanium foils are presented in Figure 4. The magnified part shows the beginning of the anodization process, where the most significant differences appear. The current-time characteristics influences the morphological properties of grown TiO_2 nanotubes which are presented in Figure 5. For the purpose of clear presentation, all the observations from Figures 4 and 5 together with the reasons for the observed behaviours are described in Table 1.

Table 1. Observed behaviour during anodic oxidation for untreated and electropolished samples.

	Untreated Samples	Electropolished Samples
Shape of the anodization curve	<ul style="list-style-type: none"> • Flat current-time curves after the steady state was reached. • A small periodic current oscillation with more intensive bubble formation (the largest impact is seen for Supplier 2). • Foil from Supplier 2 needs longer time to reach the steady-state electrical current which delayed pore formation before the nanotube growth occurs. 	A typical 3-step anodization curve corresponding to the 3 phases of the nanotube's formation process: compact oxide formation, initial porous structure formation, and nanotube growth.
	Explanation: electropolishing decreased the thickness of the starting compact oxide layer, which resulted in the faster formation of etching pits and nanotubes and an increase of current for EP samples can be seen. In case of the untreated titanium foil from Supplier 2 larger undulations and the deep pits present on the titanium foil's surface caused prolonged generation of the passive oxide layer and the formation of bubbles during the anodization which influenced the appearance of the anodized surface. The current oscillations are due to the repeated dissolution—formation of oxide layer. In contrast, the nanotubes that are grown on the electropolished titanium foil are round with smooth and thinner nanotube walls (Figure 5, Figures S4 and S5).	
Steady-state current	Less than 1 mA.	More than 1 mA.
	Explanation: a thicker oxide layer is formed at the beginning of the anodization of untreated samples with present impurities and surface defects. This thick oxide layer slows down the migration of the fluoride ions from the electrolyte, resulting in lower currents during the anodic oxidation. The smaller thickness of the compact oxide layer in EP samples caused a higher current density which promoted the growth of longer nanotubes.	
Nanotubes' shape	A hexagonal shape and ripples along the nanotube wall (Figure 5 and Figure S4).	Round with smooth and thinner nanotube walls (see Figure 5 and Figure S4).
	Explanation: ripples across the nanotube wall are due to the small periodic current oscillations during anodization.	
Nanotubes' length	Shorter (4 μm).	Longer (8 μm).
	Explanation: the growth of longer nanotubes was promoted by higher current density in case of electropolished samples. In case of untreated samples, a thinner layer of nanotubes formed under the thicker layer of the upper oxide.	

Observed behaviours are in accordance with results from the literature [22,31]. Different surface treatments of the starting titanium foils influence the amount of chemical impurities on the titanium surface and lead to a distinct electrochemical behaviour. Perillo and Rodriguez [32] performed experiments with air bubbling during the anodization process where the anodized nanotube layer showed a sponge-like porous structure with local areas of a dense, partially closed, top surface and an open tubular structure. Similar morphological characteristics were also achieved for the anodized, untreated sample from Supplier 2, as can be seen in Supplementary Figure S5. The nanotubes resulted in a dense and porous layer rather than a nanotubular layer which reduced the available active surface area for photocatalytic reaction.

Nanotubes grown on the untreated titanium foils exhibit a hexagonal shape and ripples along the nanotube wall. These are shown in Figure 5. The mentioned effect is more noticeable for the nanotubes grown by anodization of titanium from Supplier 2. In contrast, the nanotubes that are grown on the electropolished titanium foil are round with smooth and thinner nanotube walls (additional micrographs are shown in Supplementary Figure S4).

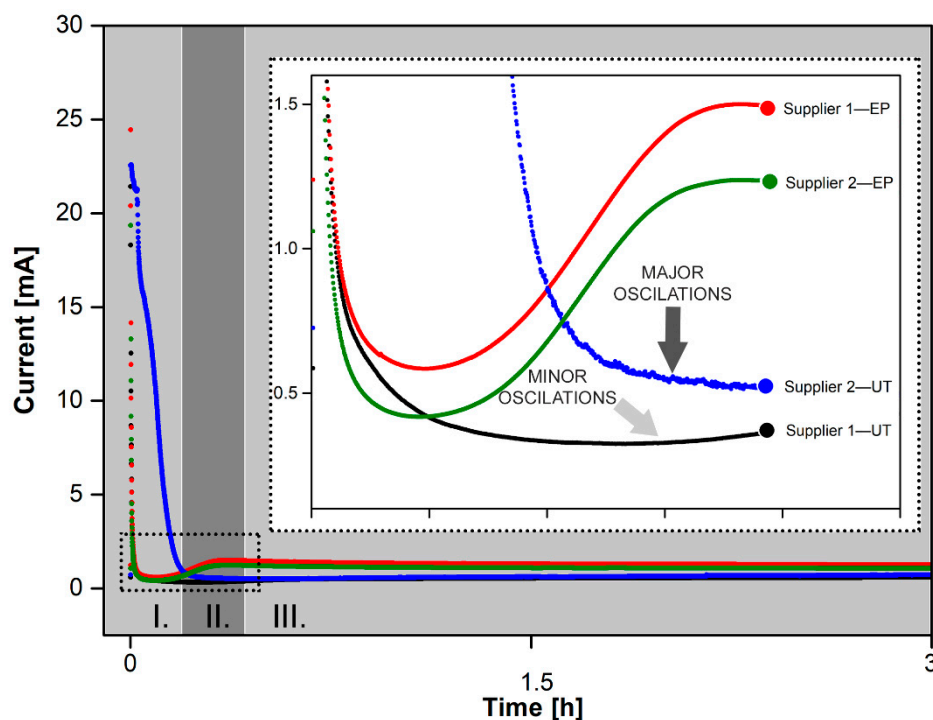


Figure 4. Current-time characteristics recorded during the anodic oxidation of the electropolished (EP) and untreated (UT) titanium foils from both suppliers. The inset shows the current at the beginning of the anodization process. Grey areas mark 3 stages of anodization curve for EP samples.

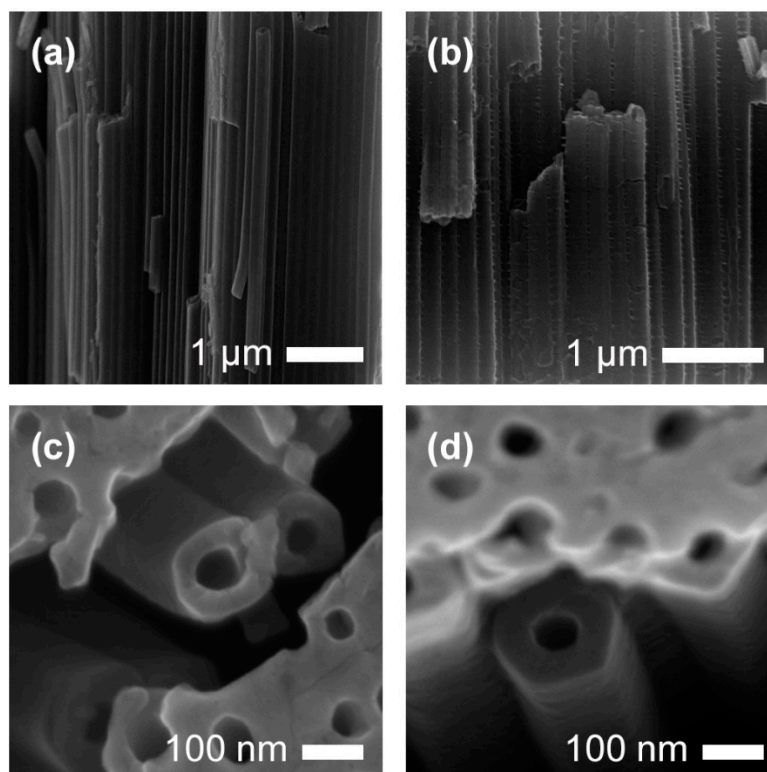


Figure 5. SEM micrographs of the anodized and annealed TiO_2 nanotubes: (a) anodized electropolished titanium with smooth nanotube wall, (b) anodized untreated titanium with ripples along the nanotube wall, (c) round-like shape grown on electropolished titanium foil and (d) hexagonal shape of TiO_2 nanotubes grown on untreated titanium foil. The same trend was observed for both suppliers.

2.3. Morphology of the TiO₂ Nanotube Arrays

Supplementary Figure S5 shows the anodized titanium foils after annealing. Considerable differences in the surface morphology can be observed between the untreated and the electropolished samples. It can be observed that the top surface of the TiO₂ nanotube layer mimics the initial surface roughness of the titanium foil and that more ordered and defect-free nanotube arrays are grown if the titanium foil is electropolished prior to the anodization. The imprints of the initial surface structural defects are more pronounced on the surface of the TiO₂ nanotube arrays of both untreated samples, where multiple steps and terraces can be seen. Supplementary Figure S8 shows topography results from 3D surface roughness mapping whereas the calculated values are shown in Table 2. Significant differences can be observed. The untreated sample from Supplier 2 exhibits the highest surface roughness of 0.632 μm, followed by the untreated sample from Supplier 1 with 0.187 μm, electropolished sample from Supplier 2 with 0.136 μm, and electropolished sample from Supplier 1 with 0.108 μm. On top of the nanotubes grown on the electropolished foils, a thinner and flatter top-oxide layer was formed. Its characteristics correspond to the appearance of the electropolished titanium foils including a thin oxide layer before anodization. Apart from that, the samples prepared with untreated foils have a higher fraction of closed nanotube tops. Cracks in the nanotube arrays can be observed for all the TiO₂ nanotube layers as a result of the annealing process in which the crystallization of the amorphous TiO₂ to the denser anatase phase occurs. The results are shown in Table 2 and the results of the nanotubular layer thicknesses and the nanotube wall thicknesses are presented in Figure 6. Those calculations were made by analyzing micrographs taken with the scanning electron microscope. Annealing of TiO₂ nanotube layers grown on the foil from Supplier 1 resulted in more dense and broader cracks in comparison to the small and curved cracks observed in the layers grown on the foil from Supplier 2. Campanelli et al. [33] attributed the cracking pattern to the existence of residual stresses during annealing. Hence, it can be assumed that the cracks appear at the locations of the grain boundaries in the titanium metal. This is also in agreement with the observations of Macak et al. [24], who observed that cracks are positioned over the grain boundaries in the titanium foil. If the cracks are wide enough for the organic molecules to traverse between them, then an additional catalytic surface area is available for the degradation reactions to occur. In our study, we noticed minor differences in the number and surface areas of the cracks between the nanotubular layers grown on the untreated and electropolished titanium foils.

Table 2. Measured and calculated pore density, cracked area and average surface roughness evaluated over the complete 3D surface of anodized untreated (UT) and electropolished (EP) titanium foils from both suppliers.

	Supplier 1—UT	Supplier 1—EP	Supplier 2—UT	Supplier 2—EP
Pore Density [%]	9.7 ± 0.6	12.7 ± 3.7	5.8 ± 2.9	10.9 ± 0.8
Cracked Area [%]	1.8 ± 0.2	4.6 ± 1.6	1.0 ± 0.3	2.5 ± 0.5
Average roughness [μm]	0.187	0.108	0.632	0.136

However, cross-sectioning of the nanotube layers showed that the nanotubes grown on the electropolished foil are more ordered, uniform, and two times longer (average length of 8 μm) than those grown on the untreated titanium foil (average length of approximately 4 μm). The nanotube arrays grown on the untreated foils show a waviness and should therefore exhibit a larger specific surface area when compared with the electropolished samples.

The nanotubes grown with anodic oxidation are amorphous and can be transformed into polycrystalline anatase nanotubes after annealing at 450 °C for 1 h. In all the samples, the characteristic peaks of tetragonal TiO₂ were detected, which correspond to the (101), (103), (004), (200), (105), (211), (204), (116), (220), and (215) anatase crystal planes (see Supplementary Figure S6). In the untreated foils, the signal from the titanium relative to the TiO₂ was higher due to the thinner TiO₂ nanotube

layer. From the relative peak-intensity values, the (101) peak appeared to be the preferred anatase crystal plane in all the samples.

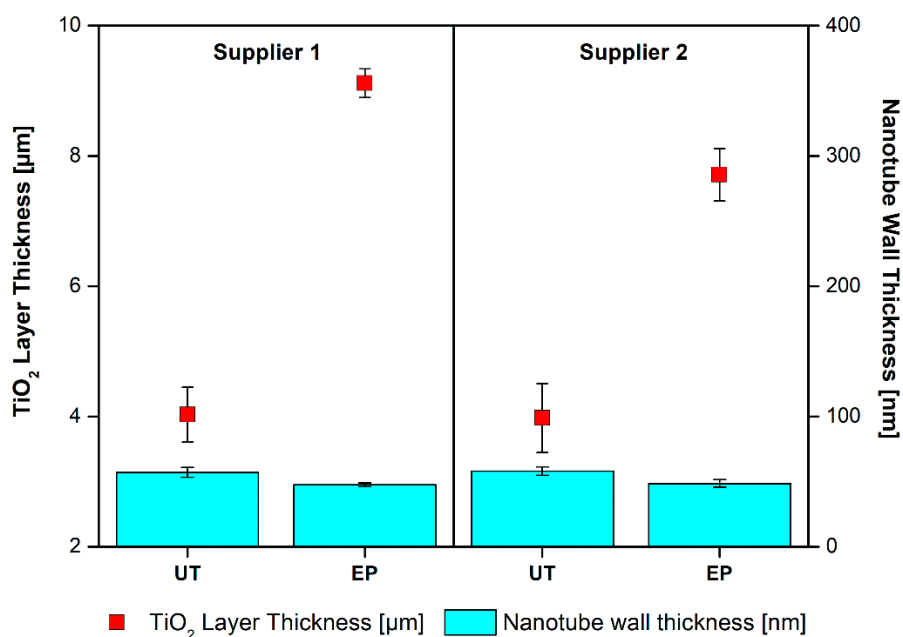


Figure 6. TiO₂ nanotube layer thickness, wall thickness and standard deviation of the results for the anodized untreated and electropolished titanium foils from both suppliers.

The TiO₂ surface composition was determined by the XPS, taking into account the relative sensitivity factors provided by the instrument manufacturer [30]. During data processing, the XPS spectra were aligned by setting the C 1s peak at 284.8 eV, characteristic for C-C/C-H bonds. On every sample, a survey spectrum over a wide energy range was acquired, as shown in Figure 7.

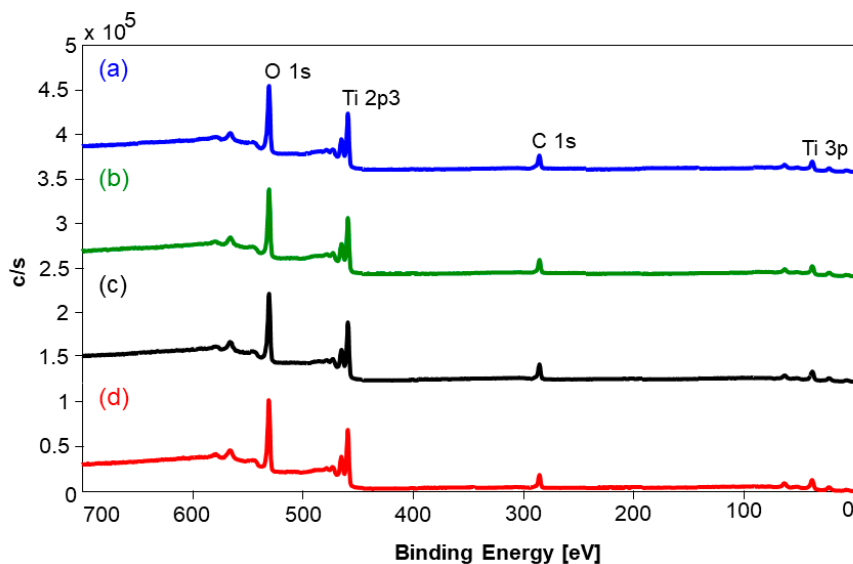


Figure 7. XPS survey spectra for (a) untreated and (b) electropolished anodized samples from Supplier 2 and (c) untreated and (d) electropolished samples from Supplier 1. The O 1s, Ti 2p₃, C 1s and Ti 3p peaks are marked.

In order to get an insight into the chemical bonding of the surface atoms, we measured high-energy resolution XPS spectra on every sample. The elements C, Ti, and O were identified on the surfaces of

all the samples, together with some traces of nitrogen. The carbon atoms probably originated from the surface contamination. The spectra are very similar and contain the O 1s, Ti 2p, Ti 3p, O KLL, and C 1s peaks. From the intensities of the O 1s, Ti 2p, and C 1s peaks, the surface concentrations were calculated. On all the samples, the chemical composition was 25–29 at. % of C, 50–52 at. % of O, and 21–23 at. % of Ti.

The Ti 2p spectrum is presented in Supplementary Figure S7a. It is composed of a doublet consisting of a Ti 2p_{3/2} peak at 458.6 eV and a Ti 2p_{1/2} peak at 464.4 eV. All the Ti 2p_{3/2} peaks are very narrow, having a full width at half maximum (FWHM) of 1.1 eV, indicating a very ordered and defect-free TiO₂ nanotube phase. The binding energy of the Ti 2p_{3/2} peak at 458.6 eV means that the Ti atoms are in the Ti⁴⁺ oxidation state in the TiO₂ nanotube. The Ti³⁺ states that should appear as a peak at about 457.5 eV were not detected in the XPS spectra. The O 1s spectrum in all the samples is relatively similar, having the main peak at 529.8 eV (Figure S7b). This peak is usually assigned to O²⁻ ions in the TiO₂ oxide matrix. All the O 1s spectra also contain a small peak at 532.0 eV. This small peak may be related either to oxygen vacancies (defects) in the TiO₂ matrix or to adsorbed OH, H₂O, C-O groups at the surface. The untreated sample from Supplier 2 has the most substantial portion of O 1s sub-peak, relatively, at 532.0 eV, and the electropolished sample from Supplier 1 has, relatively, the smallest portion of O 1s sub-peak at 532.0 eV. This sub-peak in the O 1s spectra is often correlated with the photocatalytic activity of TiO₂ nanotubes. The carbon C 1s spectra were measured, and they are presented in Supplementary Figure S7c. The main peak is at 284.8 eV, representing C-C/C-H bonded carbon atoms, probably originating from surface contamination. There is also a peak at 286.2 eV in the C 1s spectra, probably related to the C-O/C-OH bonds and the peak at 288.9 eV related either to the O-C=O groups or the CO₃ species.

2.4. Photocatalytic Degradation of the Caffeine

The photocatalytic activities of TiO₂ nanotube layers grown on four distinct titanium foil surfaces were determined with the photocatalytic degradation of caffeine as a model degradation compound. Due to the hydrophobicity of the caffeine molecule, oxidation reactions with oxygen radicals are necessary for its degradation during photocatalytic reactions [34]. Under UV illumination, OH⁻ radicals are formed at the TiO₂ nanotube surface, which attack the C₄=C₈ double bond of the caffeine. After a series of hydroxylations and oxidations, caffeine degrades into 1,3,7-trimethyluric acid [35,36]. In the experiment, each anodized titanium foil was placed in a petri dish with 5 mL of the initial caffeine solution of 10 mg/L and illuminated with UV light intensity of 3.89 mW/cm² in a sterilizer (Kambič I-265 CK UV). The total reaction time was 350 min and the degradation was determined with a UV-Vis-IR spectrometer several times throughout the entire illumination period. The caffeine degradation results are shown in Figure 8.

The degradation performance of the anodized foils decreases in the order untreated foil from Supplier 1 (100% degradation in 5.5 h), electropolished foil of Supplier 1 (99 % degradation in 5.5 h), electropolished foil of Supplier 2 (91% degradation in 5.5 h), and untreated foil of Supplier 2 (83% degradation in 5.5 h). The best photocatalytic activity achieved with the anodized untreated foil from Supplier 1 corresponds to a photonic efficiency (ξ) of 0.9% and an initial reaction rate (R_i) of 0.005 (mol L⁻¹s⁻¹) × 10⁶. The values were calculated using the equations described by Krivec et al. [37]. Whereas the results reported in the literature by different authors are difficult to compare, the comparison of the four samples tested in our study is straightforward. The differences observed can be explained with the results of the foils and the photocatalytic nanotube layers' characterization with X-ray diffraction, electron microscopy and X-ray photoelectron spectroscopy. The most noticeable difference is between the foils of different manufacturers. In the case of the foil from Supplier 1, electropolishing of the foil surface impairs the photocatalytic properties of the TiO₂ nanotube layer. The opposite is observed for the foil from Supplier 2, in which electropolishing greatly enhances the photocatalytic properties of the TiO₂ nanotube layer grown during anodic oxidation. The reason is the difference in the chemical composition of the starting titanium foils. The foil from Supplier 2 contains a higher concentration

of nitrogen present in the form of titanium nitride. The content of nitride is greatly reduced during electropolishing, which causes the growth of a higher-quality TiO₂ nanotubular layer during the anodic oxidation. Electropolishing the foil from Supplier 2 also greatly reduces the surface roughness and removes large peaks and valleys that affect the electrical current during anodization and result in the formation of a less photocatalytically active, uneven TiO₂ nanotube layer with areas of sponge-like structure. The deep valleys observed on the titanium foil of Supplier 2 impair the accessibility of these regions to fluoride ions during the anodization process, which further affects the slower dissolution of the initial oxide film present before the anodization of the foil and therefore the smaller surface area of the photocatalytically active top surface of the nanotubes. The foil from Supplier 1 contains much less nitride, and its percentage also decreases after electropolishing. In this case, it does not improve the photocatalytic properties of the grown TiO₂ nanotubular layer, since the surface roughness of the untreated foil from Supplier 1 was more suitable than that obtained after electropolishing. In addition to the roughness of the foil prior to anodizing, the photocatalytic activity of the TiO₂ nanotube layer is also affected by the nanotube wall's morphology, which is smooth in the case of the electropolished sample and bamboo-like in the case of the untreated sample. The latter has the effect of increasing the photocatalytic surface and thus the activity of the photocatalyst. In addition, the thickness of the TiO₂ nanotube layer and the smoothness of its top surface do not significantly affect its photocatalytic properties, as is often described in the literature. The TiO₂ nanotube layers that were grown on the electropolished foils are about twice as thick and have a much smoother surface, which does not necessarily mean better photocatalytic activity.

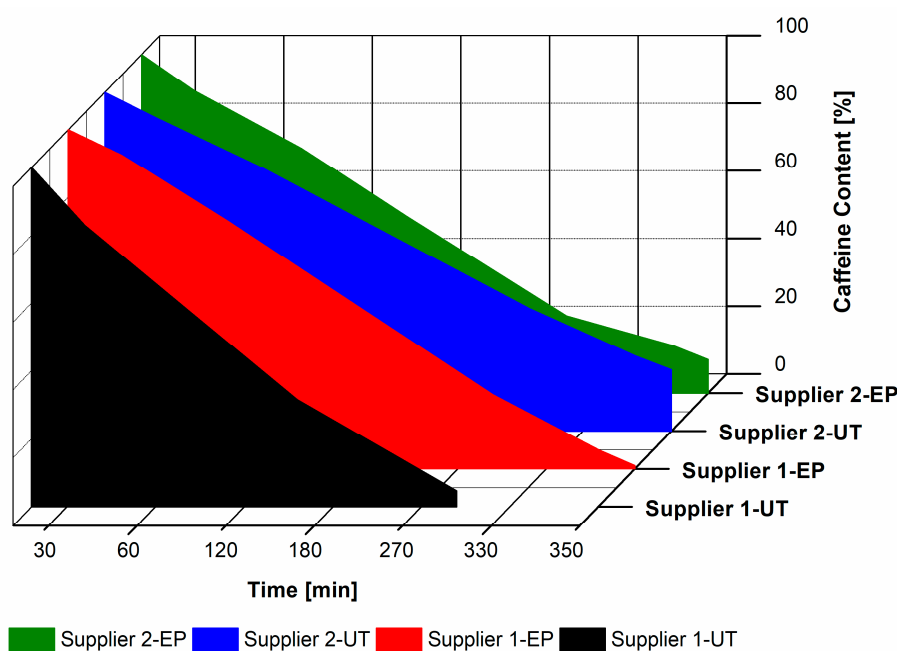


Figure 8. Photocatalytic degradation of caffeine by anodized untreated and electropolished titanium foils from both suppliers under UV irradiation. The degradation of the caffeine solution (10 ppm) was measured over a time period of 350 min. Samples were taken periodically, and the degradation was evaluated with a UV-Vis-IR spectrophotometer.

3. Materials and Methods

The study was divided into two parts. In the first part, we identified the optimum electropolishing conditions that would give a mirror-like finish on the titanium foil. In the second part, the untreated and electropolished titanium foils were anodized and their photocatalytic activity was determined. The most photocatalytically active TiO₂ nanotube arrays were then studied in detail to determine the

morphological and structural differences among them and the factors that contribute to the differences in their photocatalytic activity

3.1. Electropolishing of Titanium Foils

Titanium foils from two different suppliers, 200 μm thick, 99.9%, Baoji Lyne Metals Co., Ltd., Baoji, China (designated as Supplier 1) and 200 μm thick, 99.7%, Advent Research Materials Ltd., Oxford, UK (designated as Supplier 2) were cut into $15 \times 15 \text{ mm}^2$ samples and ultrasonically cleaned to remove impurities. Table 3 shows the chemical composition of both titanium foils as received from the manufacturers. There are different amounts of impurities present in both titanium foils. The biggest difference is the iron content. There is 0.15% Fe in the foil from Supplier 2 and only 0.05% Fe in the foil from Supplier 1. This is followed by the nitrogen content, with 0.012% in the foil from Supplier 2 and 0.005% in the foil from Supplier 1. Before anodization, some titanium foils were electropolished and some were left untreated. Electropolishing was carried out on an electrolytic polishing machine (LectroPol-5, Struers, Cleveland, OH, USA) under various conditions: temperature (10, 15, and 20 $^{\circ}\text{C}$), applied voltage (10, 30, 35, 40, and 45 V) and time of electropolishing (5, 10, 20, 30, and 60 s), using Struers A3 electrolyte (methanol, 2-butoxyethanol, and 60% perchloric acid). The same side of titanium foil was always electropolished.

Table 3. Declared chemical composition of starting titanium foils ¹.

[wt %]	Ti	Fe	C	N	H	O
Supplier 1	99.850	0.05	0.012	0.005	0.003	0.08
Supplier 2	99.663	0.15	0.02	0.012	0.005	0.15

¹ EDS analysis did not show any significant differences between both suppliers and is therefore not presented.

3.2. Microstructure and Chemical Composition of the Metal Surfaces

Chemical and microstructure characterization of titanium foils was performed to determine their surface roughness, grain size distribution, crystal structure, and the surface and subsurface chemical composition. Altogether, 27 different polishing conditions were used to polish the titanium foils from each supplier. However, only the best five polishing conditions were used for the subsequent detailed investigations. These were selected according to the appearance of the polished foils under optical stereomicroscope (Discovery V8, Carl Zeiss Microscopy GmbH, Jena, Germany). The selected foils had no visible scratches or otherwise damaged surfaces. Polished and raw titanium foils were further characterized in a field-emission gun scanning electron microscope (FSEM JSM-7600F, JEOL Ltd., Tokyo, Japan). Additionally, the topography and the surface roughness of the electropolished and untreated titanium foils were determined with a stylus profiler with a 2- μm tip (DektakXT, Bruker, Billerica, MA, USA). For the determination of the grain size distribution, electropolished samples were etched for approximately 10 min with concentrated hydrochloric acid (37%, Carlo Erba Reagents SAS, Val de Reuil, France) and thoroughly rinsed with deionized water and ethanol. After that they were observed under an optical microscope (Axio Imager Z1-m, Carl Zeiss Microscopy GmbH, Jena, Germany). Electropolished samples were etched to expose grain boundaries and to improve their visibility under an optical microscope. Etched samples had clearly visible grains on which we were able to perform statistical analysis. A complete statistical analysis of the grain size distribution was performed with the Axio Vision program (AxioVs40 V 4.8.2.0, Carl Zeiss MicroImaging GmbH, Germany, 2006–2010). Diffraction patterns of both titanium foils were investigated by XRD (X'Pert PRO, Malvern Panalytical Ltd., Malvern, UK) analysis using a Cu-K α source. The diffractograms were measured between 2 $^{\circ}$ and 100 $^{\circ}$ (X'Celerator detector) with a step of 0.034 $^{\circ}$ 2 θ over the area of 10 mm in diameter for 100 s. The phase identification was performed with the X'Pert HighScore Plus program (3.0e (3.0.5), PANalytical B.V., Almelo, The Netherlands, 30 January 2012) using the International Centre

for Diffraction Data (ICDD) PDF-4+ 2019 database. X-ray photoelectron spectroscopy (XPS) was used to characterize the surface and subsurface chemistry of the untreated and polished samples. The XPS analyses were performed on a PHI-TFA XPS spectrometer (Physical Electronics Inc., Eden Prairie, MN, USA) with an Al monochromatic X-ray source on a surface area of 0.4 mm in diameter. The analyzed depth of the XPS method is about 3–5 nm. The surface composition and the chemical bonding of the detected elements was deduced from the XPS spectra. In order to analyze the subsurface region, XPS depth profiling was performed, combining ion sputtering with Ar⁺ ions with 4-keV energy and XPS spectra acquisition. The sputtering rate was estimated to be 1.5 nm/min and a subsurface region to a depth of 10 nm was analyzed.

3.3. Anodic Oxidation of Titanium Foils

Prior to anodization, the foils were cleaned ultrasonically in acetone for 10 min, rinsed in ethanol and dried under a nitrogen stream. Electrolyte for the anodization was prepared with a mixture of 0.3 wt. % ammonium fluoride (Sigma-Aldrich, St. Louis, MO, USA) and 2 vol. % deionized water in ethylene glycol (99.99%, Sigma-Aldrich, St. Louis, MO, USA). All the experiments were carried out in a specially designed electrochemical cell (Figure 9), which was connected to a DC power supply.

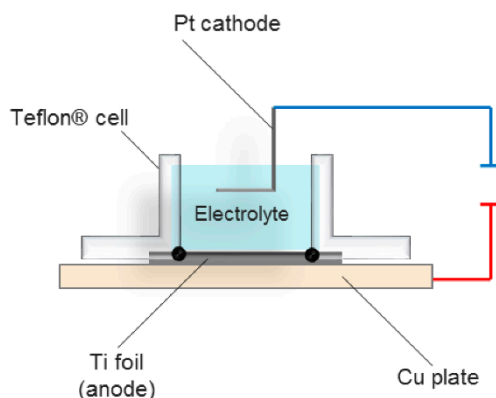


Figure 9. Electrochemical cell for anodic oxidation.

Electropolished and untreated titanium foils were anodized under a constant voltage of 60 V for 3 h using a DC power supply (TOELLNER Electronic Instrumente GmbH, Herdecke, Germany). The electrical current was monitored with a data acquisition/data logger (Agilent, Santa Clara, CA, USA). After the anodization, the titanium foils were rinsed with ethanol, dried under a nitrogen stream and annealed in air at 450 °C for 1 h (heating and cooling rates of 5 °C/min).

3.4. Characterization of the TiO₂ Nanotube Array

The morphology of the TiO₂ nanotubes was observed in a field-emission gun scanning electron microscope (FSEM JSM-7600F, JEOL Ltd., Tokyo, Japan). For the determination of the nanotubes' length, the samples were prepared by separating and crushing the nanotube layer from the titanium substrate. After placing these crushed particles on the carbon tape many situations revealed the slabs of TiO₂ nanotubes in cross-section view. The porosity and the area of the cracks in the TiO₂ nanotube array were estimated from plan-view images of the surface using the ImageJ program (ImageJ 1.52a, National Institutes of Health, United States, the program is in the public domain). Average roughness of the TiO₂ nanotube surface layers was measured with optical profiler (ZeGage™ Pro HR, Zygo Corporation, Middlefield, CT, USA) and evaluated over the complete 3D surface (Mx™ Software, Zygo Corporation, Middlefield, CT, USA). The nanotube crystallinity was investigated by XRD analysis of the immobilized annealed TiO₂ nanotube arrays, using an X'Pert PRO diffractometer (X'Pert PRO, Malvern Panalytical Ltd., Malvern, UK) with a Cu-K α source. The 2 θ angular regions between 20° and 80° were explored for 100 s (X'Celerator detector) with a step of 0.034° over an area

of 5 mm in diameter on annealed TiO₂ nanotube samples. The phase identification was performed with the X'Pert HighScore Plus program (3.0e (3.0.5), PANalytical B.V., Almelo, The Netherlands, 30 January 2012) using the International Centre for Diffraction Data (ICDD) PDF-4+ 2019 database. XPS was used to characterize the stoichiometry and oxidation states of the elements on the surfaces of the anodized TiO₂ nanotube arrays. The survey wide-energy spectrum was taken with the pass energy of the analyzer equal to 187 eV in order to identify and quantify the elements on the surface. The high-energy resolution spectrum was acquired with the energy analyzer operating at a resolution of about 0.6 eV and a pass energy of 29 eV.

3.5. Photocatalytic Degradation of the Caffeine

The photocatalytic degradation of the caffeine was measured on annealed anodized samples to determine their photocatalytic properties. Only the untreated and the most photocatalytically active electropolished (achieved with electropolishing conditions: 35 V, 30 s, 10 °C) samples from both suppliers were chosen for further testing. Titanium foils with an approximate anodized area of $0.79 \pm 0.03 \text{ cm}^2$ were placed in a petri dish with 5 mL of the initial 10 ppm caffeine solution. The solution was stirred at 250 rpm and the samples were placed in a sterilizer (I-265 CK UV, Kambič d.o.o., Semič, Slovenia) and illuminated with UV light (Ultra-Vitalux, E27, 300W, OSRAM GmbH, Munich, Germany) with intensity of 3.89 mW/cm^2 . The chosen lamp has two regions of illumination, namely UVA, from 315 to 400 nm, and UVB, from 280 to 315 nm (as provided by the supplier). After 30 min in the dark, 200 µL of caffeine solution was withdrawn and analyzed in a high-precision UV-Vis-IR spectrophotometer (Lambda 950, PerkinElmer Inc., Waltham, MA, USA). The next sample was withdrawn after the TiO₂ nanotube layer illumination for 30 min. Additional samples were later withdrawn periodically, six times over a 350-min time frame.

4. Conclusions

In summary, the anodic oxidation process was used to synthesize immobilized TiO₂ photocatalysts on untreated and electropolished titanium foils from two different suppliers. The as-purchased titanium foils varied in their chemical composition, surface roughness, and grain size distribution. These properties influenced the anodic oxidation process in which TiO₂ nanotubes with different morphology were grown. The annealed nanotube layers were characterized using FSEM, profilometry, XRD, and XPS and the photocatalytic activities for the degradation of caffeine were measured. The results presented in this paper show that the most important factor determining the photocatalytic activity is not surface morphology but, in our case, the presence of nitrides in one foil and the absence of nitrides in the other. That resulted in a significant difference because untreated titanium foil from one supplier and electropolished foil from the other supplier resulted in the best photocatalytically active samples.

Supplementary Materials: The following are available online at <http://www.mdpi.com/2073-4344/10/7/803/s1>, Figure S1: Optical microscope micrographs of chemically etched, electropolished titanium surfaces with the corresponding grain-area histogram for both titanium foil suppliers. (a) Titanium foil from Supplier 1 and (b) titanium foil from Supplier 2, Figure S2: Measured roughness factors for both titanium foil suppliers; Ra—average arithmetical roughness, Rq—root-mean-square roughness, Rt—peak-to-valley roughness, UT—untreated, EP—electropolished, Figure S3: XRD pattern for both untreated titanium foils, Figure S4: SEM micrographs of the anodized and annealed titanium foils showing (a) untreated and (b) electropolished titanium foil from Supplier 1. (c) Untreated and (d) electropolished titanium foil from Supplier 2, Figure S5: SEM images of the top surface of the annealed TiO₂ nanotube arrays. (a) Untreated and (b) electropolished titanium foil from Supplier 1. (c) Untreated and (d) electropolished titanium foil from Supplier 2, Figure S6: XRD patterns of annealed TiO₂ nanotubular layers for untreated and electropolished samples of both suppliers. Unmarked peaks correspond to the titanium foil, Figure S7: (A) Ti 2p, (B) O 1s and (C) C 1s spectrums from XPS measurement, Figure S8: Average roughness evaluated over the complete 3D surface roughness of TiO₂ nanotube layers. (a) Untreated and (b) electropolished sample from Supplier 1 and (c) untreated and (d) electropolished sample from Supplier 2 are shown. Each inset is showing a captured TiO₂ nanotube layer surface as seen through the camera on the optical profiler.

Author Contributions: Conceptualization, Ž.M. and L.S.; validation, Ž.M., L.S., Z.S., J.K., and M.Č.; investigation, Ž.M., Z.S., and J.K.; resources, Ž.M., L.S., Z.S., J.K., and M.Č.; writing—original draft preparation, Ž.M.; writing—review and editing, Ž.M., L.S., Z.S., J.K., and M.Č.; visualization, Ž.M.; supervision, M.Č.; project administration, M.Č.; funding acquisition, M.Č. All authors have read and agreed to the published version of the manuscript.

Funding: The authors gratefully acknowledge the Slovenian Research Agency (ARRS) for financial support within the research program P2-0084. This project has also received funding from the European Union's Horizon 2020 research and innovation programme under grant agreement No. 823717-ESTEEM3.

Acknowledgments: The authors would also like to thank the ULTRACOOL lab financed by Director's fund 2017 from Jožef Stefan Institute, Ljubljana for their support on working with Dektak Profilometry, CEMM team from Jožef Stefan Institute, Ljubljana for sharing their knowledge on electron microscopy and Vid Simon Šelih for his kind guidance with Zygo optical profilometry.

Conflicts of Interest: The authors declare no conflict of interest. The funders had no role in the design of the study; in the collection, analyses, or interpretation of data; in the writing of the manuscript, or in the decision to publish the results.

References

1. Ibhaddon, A.O.; Fitzpatrick, P. Heterogeneous photocatalysis: Recent advances and applications. *Catalysts* **2013**, *3*, 189–218. [\[CrossRef\]](#)
2. Hoffmann, M.R.; Martin, S.T.; Choi, W.; Bahnemann, D.W. Environmental applications of semiconductor photocatalysis. *Chem. Rev.* **1995**, *95*, 69–96. [\[CrossRef\]](#)
3. Kong, M.; Li, Y.; Chen, X.; Tian, T.; Fang, P.; Zheng, F.; Zhao, X. Tuning the relative concentration ratio of bulk defects to surface defects in TiO₂ nanocrystals leads to high photocatalytic efficiency. *J. Am. Chem. Soc.* **2011**, *133*, 16414–16417. [\[CrossRef\]](#) [\[PubMed\]](#)
4. Ge, M.; Li, Q.; Cao, C.; Huang, J.; Li, S.; Zhang, S.; Chen, Z.; Zhang, K.; Al-Deyab, S.S.; Lai, Y.; et al. One-dimensional TiO₂ nanotube photocatalysts for solar water splitting. *Adv. Sci.* **2017**, *4*, 1–31. [\[CrossRef\]](#)
5. Yu, J.; Low, J.; Xiao, W.; Zhou, P.; Jaroniec, M. Enhanced photocatalytic CO₂-Reduction activity of anatase TiO₂ by Coexposed {001} and {101} facets. *J. Am. Chem. Soc.* **2014**, *136*, 8839–8842. [\[CrossRef\]](#)
6. Bai, S.; Wang, L.; Li, Z.; Xiong, Y. Facet-engineered surface and interface design of photocatalytic materials. *Adv. Sci.* **2017**, *4*, 1–26. [\[CrossRef\]](#)
7. Roy, P.; Berger, S.; Schmuki, P. TiO₂ nanotubes: Synthesis and applications. *Angew. Chem. Int. Ed.* **2011**, *50*, 2904–2939. [\[CrossRef\]](#)
8. Ou, H.H.; Lo, S.L. Review of titania nanotubes synthesized via the hydrothermal treatment: Fabrication, modification, and application. *Sep. Purif. Technol.* **2007**, *58*, 179–191. [\[CrossRef\]](#)
9. Zhang, J.; Xiao, X.; Nan, J. Hydrothermal-hydrolysis synthesis and photocatalytic properties of nano-TiO₂ with an adjustable crystalline structure. *J. Hazard. Mater.* **2010**, *176*, 617–622. [\[CrossRef\]](#)
10. Gong, D.; Grimes, C.A.; Varghese, O.K.; Hu, W.; Singh, R.S.; Chen, Z.; Dickey, E.C. Titanium oxide nanotube arrays prepared by anodic oxidation. *J. Mater. Res.* **2001**, *16*, 3331–3334. [\[CrossRef\]](#)
11. Maiyalagan, T.; Viswanathan, B.; Varadaraju, U.V. Fabrication and characterization of uniform TiO₂ nanotube arrays by sol-gel template method. *Bull. Mater. Sci.* **2006**, *29*, 705–708.
12. Zhou, X.; Liu, N.; Schmuki, P. Photocatalysis with TiO₂ nanotubes: “Colorful” Reactivity and designing site-specific photocatalytic centers into TiO₂ nanotubes. *ACS. Catal.* **2017**, *7*, 3210–3235. [\[CrossRef\]](#)
13. Tao, J.; Zhao, J.; Tang, C.; Kang, Y.; Li, Y. Mechanism study of self-organized TiO₂ nanotube arrays by anodization. *New J. Chem.* **2008**, *32*, 2164–2168. [\[CrossRef\]](#)
14. Zhou, X.; Nguyen, N.T.; Özkan, S.; Schmuki, P. Anodic TiO₂ nanotube layers: Why does self-organized growth occur—A mini review. *Electrochem. Commun.* **2014**, *46*, 157–162. [\[CrossRef\]](#)
15. Kowalski, D.; Kim, D.; Schmuki, P. TiO₂ nanotubes, nanochannels and mesosponge: Self-organized formation and applications. *Nano Today* **2013**, *8*, 235–264. [\[CrossRef\]](#)
16. Boyjoo, Y.; Sun, H.; Liu, J.; Pareek, V.K.; Wang, S. A review on photocatalysis for air treatment: From catalyst development to reactor design. *Chem. Eng. J.* **2017**, *310*, 537–559. [\[CrossRef\]](#)
17. Lu, K.; Tian, Z.; Geldmeier, J.A. Polishing effect on anodic titania nanotube formation. *Electrochim. Acta* **2011**, *56*, 6014–6020. [\[CrossRef\]](#)

18. Hu, N.; Gao, N.; Starink, M.J. The influence of surface roughness and high pressure torsion on the growth of anodic titania nanotubes on pure titanium. *Appl. Surf. Sci.* **2016**, *387*, 1010–1020. [[CrossRef](#)]
19. Sopha, H.; Jäger, A.; Knotek, P.; Tesař, K.; Jarosova, M.; Macak, J.M. Self-organized anodic TiO₂ nanotube layers: Influence of the Ti substrate on nanotube growth and dimensions. *Electrochim. Acta* **2016**, *190*, 744–752. [[CrossRef](#)]
20. Albu, S.P.; Schmuki, P. Influence of anodization parameters on the expansion factor of TiO₂ nanotubes. *Electrochim. Acta* **2013**, *91*, 90–95. [[CrossRef](#)]
21. Pouilleau, J.; Devilliers, D.; Garrido, F.; Durand-Vidal, S.; Mahé, E. Structure and composition of passive titanium oxide films. *Mater. Sci. Eng. B* **1997**, *47*, 235–243. [[CrossRef](#)]
22. Asgari, V.; Noormohammadi, M.; Ramazani, A.; Kashi, M.A. A new approach to electropolishing of pure Ti foil in acidic solution at room temperature for the formation of ordered and long TiO₂ nanotube arrays. *Corros. Sci.* **2018**, *136*, 38–46. [[CrossRef](#)]
23. Lee, B.G.; Hong, S.Y.; Yoo, J.E.; Choi, J. Electropolishing for the formation of anodic nanotubular TiO₂ with uniform length and density. *Appl. Surf. Sci.* **2011**, *257*, 7190–7194. [[CrossRef](#)]
24. Macak, J.M.; Jarosova, M.; Jäger, A.; Sopha, H.; Klementová, M. Influence of the Ti microstructure on anodic self-organized TiO₂ nanotube layers produced in ethylene glycol electrolytes. *Appl. Surf. Sci.* **2016**, *371*, 607–612. [[CrossRef](#)]
25. Zou, J.P.; Wang, R.Z. Debonding phenomenon of TiO₂ nanotube film. *Trans. Nonferrous Met. Soc. China* **2012**, *22*, 2691–2699. [[CrossRef](#)]
26. Zou, J.P.; Wang, R.Z. Crack initiation, propagation and saturation of TiO₂ nanotube film. *Trans. Nonferrous Met. Soc. China* **2012**, *22*, 627–633. [[CrossRef](#)]
27. Baek, S.M.; Polyakov, A.V.; Moon, J.H.; Semenova, I.P.; Valiev, R.Z.; Kim, H.S. Effect of surface etching on the tensile behavior of coarse- and ultrafine-grained pure titanium. *Mater. Sci. Eng. A* **2017**, *707*, 337–343. [[CrossRef](#)]
28. Jarosz, M.; Kapusta-Kołodziej, J.; Jaskuła, M.; Sulka, G.D. Effect of different polishing methods on anodic titanium dioxide formation. *J. Nanomater.* **2015**, 1–10. [[CrossRef](#)]
29. König, U.; Davepon, B. Microstructure of polycrystalline Ti and its microelectrochemical properties by means of electron-backscattering diffraction (EBSD). *Electrochim. Acta* **2001**, *47*, 149–160. [[CrossRef](#)]
30. Moulder, J.F.; Stickle, W.F.; Sobol, P.E.; Bomben, K.D. *Handbook of X-ray Photoelectron Spectroscopy*; Chastain, J., Ed.; Physical Electronics (Perkin-Elmer Corporation): Eden Prairie, MN, USA, 1992; p. 261.
31. Xie, Z.B.; Blackwood, D.J. Effects of anodization parameters on the formation of titania nanotubes in ethylene glycol. *Electrochim. Acta* **2010**, *56*, 905–912. [[CrossRef](#)]
32. Perillo, P.M.; Rodriguez, D.F. Growth control of TiO₂ nanotubes in different physical environments. *Nanosci. Methods* **2012**, *1*, 194–200. [[CrossRef](#)]
33. Contri Campanelli, L.; Sergio Carvalho Pereira da Silva, P.; Camarinho Oliveira, N.T.; Bolfarini, C. Effect of the modification by titanium dioxide nanotubes with different structures on the fatigue response of Ti grade 2. *Mater. Res.* **2017**, *20*, 120–124. [[CrossRef](#)]
34. Tavagnacco, L.; Schnupf, U.; Mason, P.E.; Saboungi, M.-L.; Cesàro, A.; Brady, J.W. Molecular dynamics simulation studies of caffeine aggregation in aqueous solution. *J. Phys. Chem. B* **2011**, *115*, 10957–10966. [[CrossRef](#)] [[PubMed](#)]
35. Dalmázio, I.; Santos, L.S.; Lopes, R.P.; Eberlin, M.N.; Augusti, R. Advanced oxidation of caffeine in water: On-line and real-time monitoring by electrospray ionization mass spectrometry. *Environ. Sci. Technol.* **2005**, *39*, 5982–5988. [[CrossRef](#)]
36. Telo, J.P.; Vieira, A.J.S.C. Mechanism of free radical oxidation of caffeine in aqueous solution. *J. Chem. Soc. Perkin. Trans.* **1997**, *2*, 1755–1757. [[CrossRef](#)]
37. Krivec, M.; Žagar, K.; Suhadolnik, L.; Čeh, M.; Dražić, G. Highly efficient TiO₂-based microreactor for photocatalytic applications. *ACS. Appl. Mater. Interfaces* **2013**, *5*, 9088–9094. [[CrossRef](#)]

